

No facilitator required for membrane transport of hydrogen sulfide

John C. Mathai^{a,1}, Andreas Missner^{b,1}, Philipp Kügler^{c,d}, Sapar M. Saparov^b, Mark L. Zeidel^a, John K. Lee^e, and Peter Pohl^{b,2}

^aBeth Israel Deaconess Medical Center and Harvard Medical School, 330 Brookline Avenue, Boston, MA 02215; ^bInstitut für Biophysik and ^cIndustrial Mathematics Institute, Johannes Kepler Universität Linz, Altenbergerstrasse 69, A-4040 Linz, Austria; ^dJohann Radon Institute for Computational and Applied Mathematics, Austrian Academy of Sciences, Altenbergerstrasse 69, A-4040 Linz, Austria; and ^eDepartment of Biochemistry and Biophysics, University of California, San Francisco, CA 94158

Edited by Francisco Bezanilla, University of Chicago, Chicago, IL, and approved July 27, 2009 (received for review March 17, 2009)

Hydrogen sulfide (H₂S) has emerged as a new and important member in the group of gaseous signaling molecules. However, the molecular transport mechanism has not yet been identified. Because of structural similarities with H₂O, it was hypothesized that aquaporins may facilitate H₂S transport across cell membranes. We tested this hypothesis by reconstituting the archeal aquaporin AfAQP from sulfide reducing bacteria *Archaeoglobus fulgidus* into planar membranes and by monitoring the resulting facilitation of osmotic water flow and H₂S flux. To measure H₂O and H₂S fluxes, respectively, sodium ion dilution and buffer acidification by proton release (H₂S ⇌ H⁺ + HS⁻) were recorded in the immediate membrane vicinity. Both sodium ion concentration and pH were measured by scanning ion-selective microelectrodes. A lower limit of lipid bilayer permeability to H₂S, $P_{M,H_2S} \geq 0.5 \pm 0.4$ cm/s was calculated by numerically solving the complete system of differential reaction diffusion equations and fitting the theoretical pH distribution to experimental pH profiles. Even though reconstitution of AfAQP significantly increased water permeability through planar lipid bilayers, P_{M,H_2S} remained unchanged. These results indicate that lipid membranes may well act as a barrier to water transport although they do not oppose a significant resistance to H₂S diffusion. The fact that cholesterol and sphingomyelin reconstitution did not turn these membranes into an H₂S barrier indicates that H₂S transport through epithelial barriers, endothelial barriers, and membrane rafts also occurs by simple diffusion and does not require facilitation by membrane channels.

aquaporins | gas transport | membrane permeability | unstirred layer | signaling

Hydrogen sulfide (H₂S) has emerged as a new gaseous signaling molecule despite its reputation as a toxic gas with a repulsive odor (1). H₂S is engaged in regulation and modulation of physiological functions such as vasorelaxation, vasodilatation, blood pressure modulation, and inhibition of apoptosis in a number of cell types (2–5). It is an important mediator of endotoxemic shock (6) and acute inflammation, acting at the leukocyte–endothelium interface (7). Physiological concentrations of H₂S selectively enhance NMDA receptor-mediated responses and may modulate synaptic activities regulated by steroid hormones and neurotransmitters, suggesting that endogenous H₂S functions as a neuromodulator in the brain (8). In the brain and the vasculature, micromolar quantities of H₂S are produced by enzymes of the cysteine biosynthetic pathway (9, 10). H₂S is believed to act as a gaseous messenger like nitric oxide (NO) and carbon monoxide (CO). Unlike NO and CO, H₂S is not known to form toxic metabolites (11). Although the importance of H₂S in brain, vascular, and cardiac functions are known and new targets of its action are emerging, the transport physiology of H₂S is not well characterized.

According to some reports, H₂S is believed to be a highly lipophilic molecule and to freely penetrate cells of all types (12). According to another report, H₂S is highly soluble in water. Bubbling of H₂S into water yields a saturated solution of 100 mM H₂S (13). To the best of our knowledge, however, neither the

partition coefficient into the organic phase nor its actual membrane permeability, P_M , is known. Unfortunately, in silico predictions of the octanol water partition coefficient are not very reliable for small molecules (compare Table 1). Moreover, the structural similarity between H₂S and H₂O suggests that caution is required when applying the solubility model to predict P_M (14), meaning that even when the partition coefficient is known, the actual and predicted P_M may not match each other. The similarity between H₂S and H₂O also suggests that H₂S transport may be facilitated by water channels (15). Aquaporin-M (AqpM) an archeal water channel from *Methanothermobacter marburgensis* was speculated to provide a H₂S permeation pathway. Its crystal structure revealed a pore geometry that would easily accommodate H₂S (15). An evolutionarily close relative of AqpM, the archeal aquaporin from a sulfide-reducing bacteria *Archaeoglobus fulgidus* (AfAQP), shares 71% sequence identity with AqpM (compare *SI Text* for AfAQP sequence). In addition, the pore-forming amino acids in both of these aquaporins are identical except for replacement of cysteine-79 of AqpM with alanine in AfAQP (16). The likelihood of AfAQP being an H₂S pathway is high because aquaporin-mediated facilitation of water movement through the lipid matrix seems to be a superfluous luxury in hot springs. In contrast, temperature-mediated elevation of metabolic rates results in intracellular accumulation of H₂S, which should be toxic to the bacteria if not immediately exported. With this point in mind, we took AfAQP as the most likely H₂S channel prototype and evaluated the potential contribution of this aquaporin to H₂S membrane transport. In light of the emerging importance of H₂S as a third gaseous messenger molecule, the results should have implications for studying signal cascades in the cardiovascular system and the brain, where human aquaporins like aquaporin-1 and aquaporin-4 may act as H₂S transporters.

Aquaporins have already been reported to act as an important pathway for volatile solutes (17). Although there is little doubt that they facilitate the membrane transport of NH₃ (18), the contribution of aquaporins to NO, CO₂, or O₂ transport is under debate (19–23). At the same time as the permeability of $P_{M,CO_2} = 3.2$ cm/s allows CO₂ to pass membranes freely (22), the NH₃ permeability $P_{M,NH_3} = 0.016$ cm/s (24) indicates that a cholesterol-containing epithelial membrane acts as a barrier and, consequently, that membrane channels (aquaporin-8) facilitate NH₃ diffusion (18). The different findings for NH₃ and CO₂ are in agreement with Overton's rule (25, 26) which, based on the biphasic partition coefficients (Table 1) predicts the large difference in P_M .

Author contributions: J.C.M. and P.P. designed research; J.C.M., A.M., S.M.S., and J.K.L. performed research; P.K. contributed new reagents/analytic tools; J.C.M., A.M., S.M.S., and P.P. analyzed data; and J.C.M., A.M., M.L.Z., and P.P. wrote the paper.

The authors declare no conflict of interest.

This article is a PNAS Direct Submission.

¹J.C.M. and A.M. contributed equally to this work.

²To whom correspondence should be addressed. E-mail: peter.pohl@jku.at.

This article contains supporting information online at www.pnas.org/cgi/content/full/0902952106/DCSupplemental.

Table 1. Predicted and measured octanol water partition coefficients for different volatile molecules

Volatile molecule	Predicted partition coefficient	Measured partition coefficient
Oxygen (O ₂)	$K_{p_{O_2}}^{\dagger} = 0.08$	$K_{p_{O_2}}^{\ddagger} = 2$ (35, 36)
Ammonia (NH ₃)	$K_{p_{NH_3}}^{\dagger} = 0.2$	$K_{p_{NH_3}} = 0.002$ (29)
Carbon dioxide (CO ₂)	$K_{p_{CO_2}}^{\dagger} = 7.9$	$K_{p_{CO_2}} = 1.5$ (43)
Hydrogen sulfide	$K_{p_{H_2S}}^{\dagger} = 3.2$	Unknown

[†]Taken from the PubChem database.

[‡]Partition into the hydrophobic core of lipid membranes.

If H₂S passes membranes as fast as CO₂, ¹O₂ or O₂, its transport may actually be rate-limited by diffusion across so-called unstirred layers (USL) which are always present adjacent to membranes (27, 28). As transport across these stagnant water layers strictly occurs by diffusion, the H₂S concentrations in the immediate membrane vicinity and in the bulk solution differ from one another. If not taken into account, this polarization hampers proper determination of P_M .

The near-membrane solute polarization can be measured via SEM (28). An ion-sensitive microelectrode is moved toward the planar bilayer while recording the tiny concentration changes that accompany molecule diffusion through both USLs and the planar membrane. In the absence of a H₂S electrode, a pH-sensitive microelectrode may instead be used, because at pH 7.4 the weak acid H₂S ($pK_a = 6.89$) acidifies the receiving compartment and augments pH in the donating compartment (compare Fig. 1). The spatially resolved steady-state pH shift within the USL enables determination of P_{M,H_2S} . We used an analytical model for this analysis which takes into account all relevant proton transfer reactions, including proton uptake and release by buffer molecules and the diffusion of all reactants (see *Appendix*).

Results

Hydrogen sulfide flux was induced by addition of NaHS to one side of the planar membrane, which is subsequently referred to as the *cis* side. To permeate the membrane, HS⁻ has to pick up a proton at

the *cis* membrane–water interface and to release a proton at the opposite (*trans*) interface. The resulting acidification in the *trans* USL was measured by a scanning pH microelectrode. As the H₂S concentration increased, the pH shift within the *trans* USL also increased (Fig. 2A).

To obtain P_M , the set of differential equations comprising our analytical model was fitted to the first 50 μm of the experimentally obtained pH profiles. The value of 0.05 cm/s represents the smallest P_M for which a satisfactory fit was obtained. Calculation for $P_M > 0.05$ cm/s resulted in theoretical pH profiles, which were indistinguishable from those obtained for $P_M = 0.05$ cm/s. This observation indicates (i) that the value of 0.05 cm/s represents only the lower limit of P_M , and (ii) that the limiting step of H₂S transport across the planar bilayer is its diffusion through the USLs. The latter conclusion is illustrated by the plot of the corresponding theoretical H₂S concentration profiles (Fig. 2B). They show that more than 99% of the H₂S gradient is lost within the USLs.

A more precise determination of P_M requires that permeation through the membrane be the rate-limiting step. As the concentration of the neutral species is pH-dependent, the rate-limiting step is expected to be a function of bulk pH, too. In contrast to USLs, which limit transport at neutral pH, the membrane may be rate-limiting at basic pH, as has been previously proven for other weak acids (29, 30). The switch in the limiting step may occur because (i) the total flux is much smaller at pH 8.9, as 98% of the weak acid H₂S is charged, and (ii) the transmembrane flux affects the H₂S concentration adjacent to the membrane to a much lower extent than the extremely fast proton uptake which constantly replenishes H₂S. However, P_M appeared to be so large that the above-mentioned mechanisms were insufficient to transform diffusion through the membrane into the rate-limiting step. The best fit of the analytical model to near-membrane pH profiles measured at various H₂S concentrations revealed $P_M \geq 0.5$ cm/s (Fig. 3A). Calculation of the corresponding H₂S concentration profile showed that the main resistance to H₂S diffusion was still generated by USLs (Fig. 3B).

Because USLs adjacent to vascular endothelia are at least an order of magnitude smaller than those adjacent to planar bilayers,

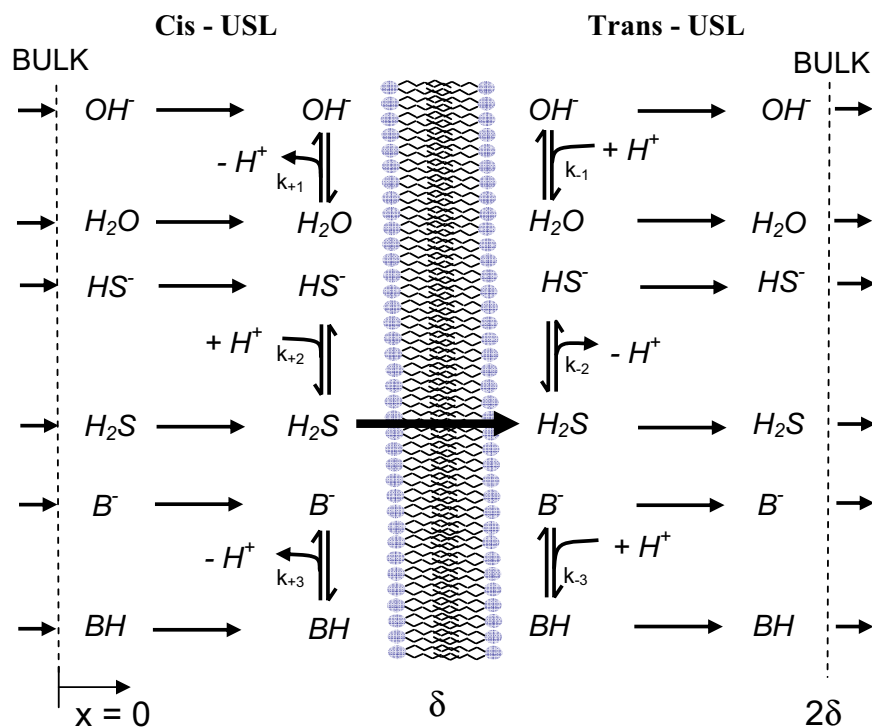


Fig. 1. Scheme of H₂S transport across lipid membranes. δ denotes the size of the unstirred layer (USL) present on both sides. Transport of H₂S across a membrane includes four steps: (i) all participating molecules (protonated and deprotonated forms) diffuse from the *cis* bulk to the membrane; (ii) at the membrane surface, HS⁻ gets protonated; (iii) only the uncharged form of hydrogen sulfide (H₂S) permeates the membrane; (iv) after passing the membrane, most of the H₂S molecules release a proton; and (v) all molecules diffuse from the membrane to *trans* bulk. The presence of buffer molecules (B⁻, BH) is essential for providing stable bulk.

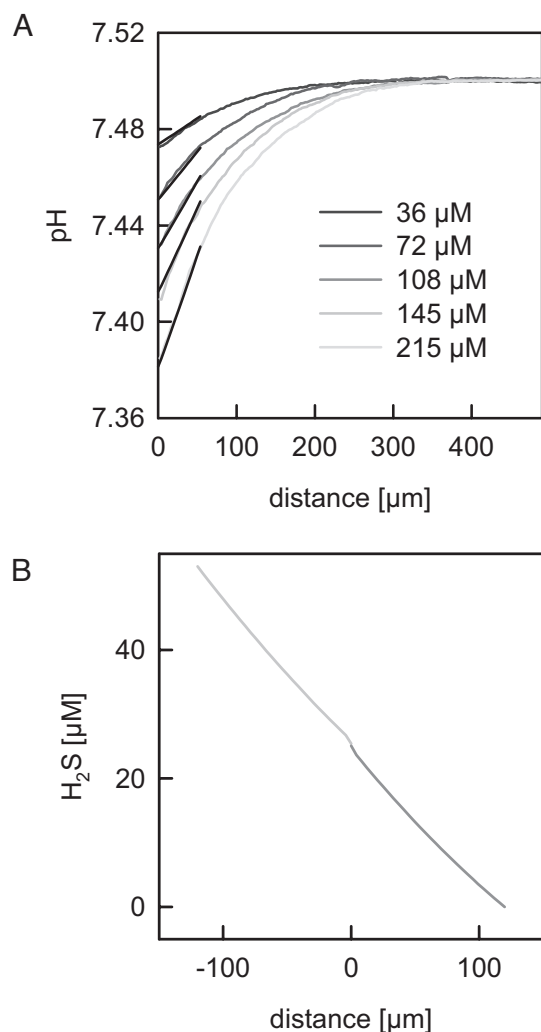


Fig. 2. Near-membrane pH and H₂S concentration distributions for bulk pH 7.4. (A) Experimental pH profiles (bulk pH = 7.5) in the *trans* unstirred water layer. A H₂S gradient was induced by different NaHS concentrations (as indicated) in the *cis* compartment. Increasing H₂S gradients resulted in an increased proton accumulation in the *trans* unstirred layer. The analytical model was fitted to the first 50 μm of the experimental pH profiles. The best fit resulted in $P_{M,H_2S} = 0.05$ cm/s (black lines). The bathing solution contained 100 mM NaCl and 5 mM Mops adjusted to pH = 7.5. (B) The analytical model (see *Appendix*) allowed visualization of the corresponding H₂S concentration distributions in the *cis* and *trans* USLs. As an example, the concentration profiles for the HS⁻ bulk concentration of 215 μM is shown. The lack of a transmembrane H₂S gradient indicates that membrane resistance to H₂S diffusion is negligible.

we calculated the contribution a 1-μm thick USL would offer to H₂S membrane resistance. By solving the differential equations (see *Appendix*), we found that such an extremely thin USL accounts for ≈80% of the total membrane resistance to H₂S (Fig. 4). This value decreases to 50% for $\delta \approx 300$ nm. That is, at room temperature AfaAQP may double H₂S membrane permeability if present at high surface density. At 80 °C—i.e., at temperatures comparable with those at which the *A. fulgidus* cytoplasmic membrane is physiologically exposed—the USL contributes more than 95% to the total resistance (Fig. 4), and AfaAQP cannot significantly contribute to H₂S membrane permeability.

Bilayer tightening by cholesterol and sphingomyelin decreases the diffusivity of small molecules, thereby increasing membrane resistance. For example, bilayer tightening decreases membrane permeability to water by up to tenfold (31, 32) and to ammonia by threefold (24). However, cholesterol- and sphingomyelin-

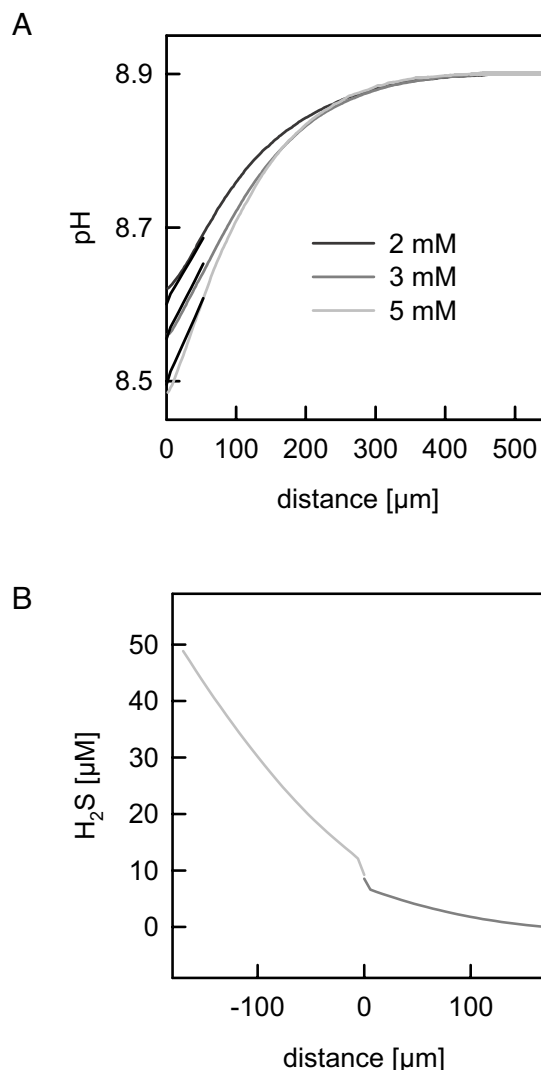


Fig. 3. Near-membrane pH and H₂S concentration distributions for bulk pH 8.9. (A) Representative recordings of the acidification in the *trans* unstirred layer at different NaHS concentrations in the *cis* compartment. The bulk solutions contained 100 mM NaCl and 5 mM Tris adjusted to pH = 8.9. The black lines represent the best fit of the analytical model to the experimental profiles ($P_{M,H_2S} = 0.5$ cm/s). (B) Corresponding theoretical H₂S profiles are shown in the *cis* and *trans* USLs for a membrane permeability $P_{M,H_2S} = 0.5$ cm/s (bulk HS⁻ concentration 5 mM). Even at pH = 8.9, the USLs in the immediate membrane vicinity are rate-limiting to the H₂S transport process.

containing bilayers had the same H₂S permeability of $P_M \geq 0.5$ cm/s (Fig. 5), indicating that the membrane is not the limiting factor in H₂S transport regardless of membrane composition.

If the resistance of the membrane to H₂S flux is negligibly small, reconstitution of H₂S-conducting channels should not alter this flux. We checked this hypothesis by reconstituting purified AfaAQP into planar lipid membranes. The membranes were folded from monolayers on top of a proteoliposome suspension (33, 34) prepared from a natural mixture of *Escherichia coli* lipids. As anticipated, near-membrane acidification generated by a transmembrane H₂S gradient was insensitive to the presence of AfaAQP (Fig. 5). This result further confirmed that bilayer background conductivity was larger than any incremental conductivity that AfaAQP might have introduced into the membrane.

AfaAQP was fully functional in our planar bilayers, as revealed by water-flux measurements (Fig. 6). Addition of 1 M urea into the *cis* compartment resulted in dilution of sodium ions adjacent to the

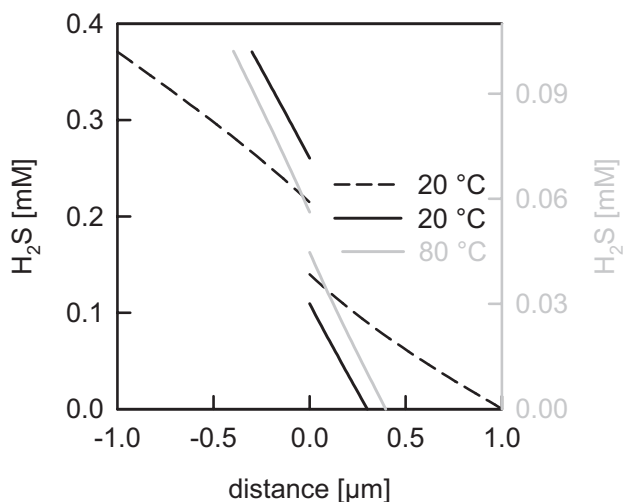


Fig. 4. Calculated H_2S profiles for size-reduced USLs at 20 °C and 80 °C. The total bulk concentrations of the weak acid ($\text{H}_2\text{S} + \text{HS}^-$) were set to 1 mM (*cis*) and 0 mM (*trans*) compartments. The differential equations were solved for $\delta = 0.3$ and 1 μm (20 °C). For the calculation at 80 °C, we took into account the following: (i) the different H_2S diffusion coefficients of 2 and $4.62 \times 10^{-5} \text{ cm}^2/\text{s}$ at 20 °C and 80 °C, respectively (46); (ii) the increase of the diffusion coefficients of all other substances by a factor of 3.4; (iii) the decrease of pK of H_2S from 6.89 to 6.33; (iv) the increase of δ from 300 to 396 nm [δ scales with the third root of D (28)]; and (v) a tenfold-increased H_2S permeability from $P_{f,\text{H}_2\text{S}} = 0.5 \text{ cm/s}$ at 20 °C to $P_{f,\text{H}_2\text{S}} = 5 \text{ cm/s}$ at 80 °C. Comparison with the increase in water permeability (Arrhenius plot) shows that this factor is most likely an underestimation. Nevertheless, more than 95% of the H_2S gradient is lost within the stagnant water layers next to the membrane. If at 80 °C, $P_{f,\text{H}_2\text{S}} > 5 \text{ cm/s}$, the USL would account for more than 95% of the resistance to H_2S flow. Thus, facilitated H_2S transport is very unlikely, especially at elevated temperatures.

membrane. Measurements gathered by scanning sodium micro-electrodes demonstrated a larger sodium-concentration drop for membranes containing the water channel AfAQP as compared with bare membranes. The osmotic permeabilities in the presence and the absence of AfAQP were $41 \pm 3 \mu\text{m}$ and $23 \pm 2 \mu\text{m/s}$, respectively. We have also carried out stopped-flow measurements

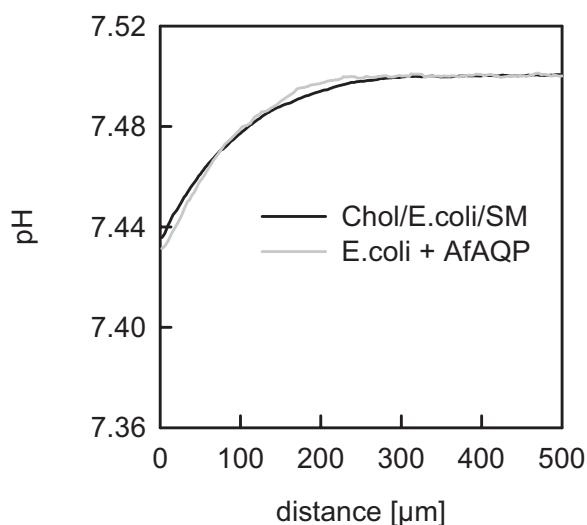


Fig. 5. Experimental pH profiles induced by H_2S flux from *cis* to *trans* side at a bulk pH equal to 7.5. The pH changes did not significantly differ from those measured for sphingomyelin and cholesterol (cholesterol:*E. coli* lipid:sphingomyelin = 3:2:1 by mass) containing membranes and *E. coli* lipid bilayers reconstituted with AfAQP (mass ratio of 1:75).

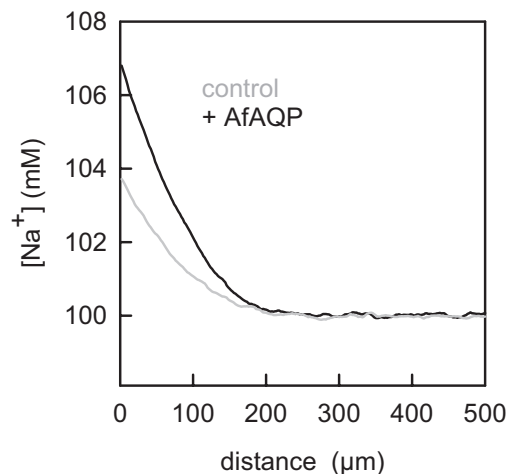


Fig. 6. Representative concentration profiles showing that osmotic water flow is accompanied by sodium retention at the hypotonic side of the lipid bilayer. The hyperosmotic compartment contained 1 M urea. Water permeability was $P_f = 23 \pm 2 \mu\text{m/s}$ for the bare lipid bilayer and increased to $P_f = 41 \pm 3 \mu\text{m/s}$ after AfAQP reconstitution at a protein:lipid mass ratio of 1:75. Buffer solution contained 100 mM NaCl and 5 mM Mops, pH = 7.5.

to visualize the rate at which proteoliposomes shrink when exposed to a hyperosmotic solution (Fig. S1). From the temperature dependence, we calculated that the activation energy for water flow through AfAQP amounts to 4.5 kcal/mole (Fig. S2).

Discussion

We have shown that membrane resistance to H_2S permeation is negligible. Near-membrane USLs generate the major resistance to H_2S transport. As a consequence, we were only able to determine the lower boundary of H_2S permeability: P_M is larger than $0.5 \pm 0.4 \text{ cm/s}$. P_M is thus approximately sixfold smaller than CO_2 membrane permeability (22) and from threefold to 50-fold smaller than singlet oxygen and oxygen permeabilities (23, 35, 36), but at least an order of magnitude larger than NH_3 permeability (18, 24).

Because of the large H_2S background membrane permeability, a physiologically important contribution of aquaporins to H_2S transport is very unlikely, a point that holds true even when considering that the unique structure of archaeobacterial lipids lowers H_2S permeability. For example, archaeobacterial lipids reduce NH_3 permeability by six- to tenfold (37), i.e., to an extent similar to cholesterol and sphingomyelin (31). Our experiment reveals an unmodified H_2S permeability in the presence of cholesterol and sphingomyelin (Fig. 5), indicating that facilitation of transport by membrane channels is physiologically meaningless. The failure to observe facilitation of transmembrane H_2S diffusion by AfAQP (Fig. 5) is in line with this conclusion.

At physiological pH, the acid–base equilibrium of CO_2 and of NH_3 is very much shifted to the charged forms HCO_3^- and NH_4^+ , respectively. In contrast, approximately one third of H_2S exists as a neutral molecule and two thirds as the hydro sulfide anion as indicated by the pK value of 6.89. Consequently, if it exists at all, transport of HS^- by Cl^- channels or other anion channels is not likely to play a physiologically relevant role. The flux J_C through these channels would be negligible, as can be shown by a simple analysis of the ordinary flux equation

$$J = J_L + J_c = -P_L A_L ([\text{H}_2\text{S}]_{cis} - [\text{H}_2\text{S}]_{trans}) - P_C A_C ([\text{HS}^-]_{cis} - [\text{HS}^-]_{trans}) \quad [1]$$

where A_c , A_L , J , and J_L are the area occupied by all anion channels, the area of the lipid pathway, the total flux, and the flux through the

lipid matrix, respectively. $[HS^-]_{cis}$ and $[HS^-]_{trans}$ denote the HS^- concentrations at both sides of the membrane. For pH 7.4, we can simplify the equation to

$$\frac{J}{([H_2S]_{cis} - [H_2S]_{trans})} \approx -P_L A_L - 2P_C A_C \quad [2]$$

Substituting $P_C A_C$ for turnover number per channel T and number of anion channels m_{A^-} , we arrive at

$$\frac{J}{([H_2S]_{cis} - [H_2S]_{trans})} \approx -P_L A_L - 2m_{A^-} \frac{TV_{HS^-}}{N_A} \quad [3]$$

where V_{HS^-} and N_A are the molecular volume of HS^- and Avogadro's number, respectively. Because (i) the conductivity of a Cl^- channel is usually miniscule (<10 pS)—that is, because $T < 10^7$ s^{-1} —and (ii) $A_C m_{A^-} < 2,000$ channels μm^{-2} , and (iii) $A_L > A_C$, Eq. 1 simplifies to

$$J \approx J_L \quad [4]$$

In the absence of any function in H_2S transport, the only major remaining function of AFAQP is water transport. However, calculations of osmotic water permeability (P_f) reveal that equilibration of osmotic pressure gradients through the membrane of *A. fulgidus* should be fast even in the absence of AFAQP. Assuming that the cells are perfect spheres so that their initial volume V_0 and surface A_0 can be calculated from the diameter (d) of 600 nm (38):

$$\frac{dV(t)}{V_0 dt} = \frac{P_f A_0}{V_0} * V_w * \left[\frac{V_0 c_{in}}{V(t)} - c_{out} \right] \quad [5]$$

Assuming a P_f of 20 $\mu m/s$, we arrive at a time constant τ of ≈ 700 ms, provided that the dependence of volume on time can be described by a single exponential. Even a fivefold increase in P_f due to AFAQP functioning would result in $\tau \approx 140$ ms. It is questionable whether this gain in water-transport rate provides a benefit in nature's selection process. The question mark on its physiological significance becomes even larger if we take into account that P_f of the lipid matrix at ambient temperatures as found in hot springs is, most probably, much higher. If we assume that the temperature dependence measured for *E. coli* lipids (33) holds, P_f would be elevated to ≈ 200 $\mu m/s$ at 50 °C. To double P_f , aquaporins exhibiting a single-channel permeability, p_f , of $\approx 1 \times 10^{-14}$ cm/s at 23 °C and having an activation energy of 4.5 kcal/mol (Fig. S2) would have to be present at a density of 7,000 channels per μm^2 . Such a scenario is very unlikely because even in an aquaporin-rich tissue, such as that of red cells, the density is only $\approx 1,500$ copies/ μm^2 .

It could be argued that P_f of the archeal lipids may be very different from the P_f of *E. coli* lipids used in the present study. However, with ≈ 20 $\mu m/s$ at room temperature, planar bilayers made of diphytanoyl lipids (39) have a P_f very close to planar bilayers from *E. coli* lipids (33, 34). Even in the case of liposomes made of tetraether lipids (archaea), which exhibit very low water permeability, the estimated permeability at its ambient growth temperature is ≈ 140 $\mu m/s$ (37). Moreover, the main determinant for water flow through lipid bilayers has been shown to be the area per lipid (40, 41) and this parameter is similar for archeal lipids and those used in this study.

The argument that the single-channel permeability of AFAQP is exceptionally large does not hold either. As a simple calculation reveals, p_f is $\approx 50\%$ of that determined for aquaporin-Z in similar experiments (33): P_f is equal to the absolute hydraulic conductivity of all channels divided by the number of channels, n ; n is anticipated to be equal to the total number of lipid molecules, L , in the bilayer divided by the molar lipid-to-protein ratio, r :

$$p_f = P_f A/n = P_f A r/2L = P_f b r/2 \quad [6]$$

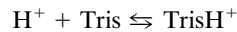
L is derived from two times the membrane area, A (because the membrane has two leaflets), divided by the area per lipid molecule, b . Assuming protein incorporation of $\approx 50\%$ efficiency (42), p_f was calculated to be 1×10^{-14} cm³/subunit/s. Thus, expression of AFAQP is unlikely to increase water flux through the archea in a hot spring. We conclude that the actual function of AFAQP still remains to be identified. The same holds for the homologous protein, aquaporin (AQPM) from *M. marburgensis*.

Similar to CO_2 and O_2 , H_2S partitions so easily into the hydrophobic core of the membrane that an aqueous pathway does not lower its energy barrier for membrane transport. NH_3 remains the only volatile molecule that is transported by an aquaporin (18). In contrast to CO_2 and O_2 , NH_3 has a partition coefficient strongly favoring the aqueous over the hydrophobic environment (29, 35, 43). Consequently, the energy barrier for diffusion through phosphatidylcholine membranes increases to an extent at which it roughly matches the barrier required for the passage of an aqueous channel (20). NH_3 transport through aquaporins becomes favorable only if the lipid barrier is increased by adding cholesterol or cholesterol and sphingomyelin (18). In contrast, the barrier for CO_2 , O_2 , and H_2S transport through the lipid core of the membrane is always lower than the barrier provided by an aqueous channel.

Appendix. In an aqueous environment H_2S is a weak acid (pK = 6.89), which dissociates according to (compare Fig. 1):



For the analytical description of the coupled reaction diffusion system, the subsequent buffer reactions (pK_{Tris} = 8.2, pK_{Mops} = 7.14):



and water hydrolysis also have to be taken into account. Similar to previously published models of weak acid transport (22, 30), a set of coupled differential equations (based on Fick's first and second laws) was solved numerically to derive the local steady-state concentrations of all reactants within the USLs:

$$J_i^{cis}(x) = -D_i \frac{dc_i^{cis}(x)}{dx} \quad R_i(c^{cis}(x)) = \frac{dJ_i^{cis}(x)}{dx} \quad [7]$$

$$J_i^{trans}(x) = -D_i \frac{dc_i^{trans}(x)}{dx} \quad R_i(c^{trans}(x)) = \frac{dJ_i^{trans}(x)}{dx} \quad [8]$$

with J_i , D_i , and c_i being the flux, diffusion constant, and concentrations, respectively, of the i th species in the *cis* and *trans* USLs adjacent to the membrane. The index i is assigned to 1 = H^+ , 2 = OH^- , 3 = B (B denotes either Tris or Mops⁻), 4 = BH (BH denotes either TrisH⁺ or MOPSH), 5 = H_2S , 6 = HS^- , and 7 = H_2O . R_i indicates the specific local rates of expenditure of corresponding chemical reactions.

All association rates, k_a , were assumed to be $\geq 2 \times 10^{10}$ dm³ mol⁻¹ s⁻¹ (44). The dissociation rates, k_d , were calculated from the respective equilibrium constants ($K_i = 10^{-pK_i} = k_d/k_a$) (30). At the water-bilayer phase boundary, all fluxes are required to be zero except for J_5 , thus allowing calculation of H_2S membrane permeability by

$$P_{M,H_2S} = \frac{J_{5,M}}{(c_{5(\alpha=\delta)}^{cis} - c_{5(\alpha=\delta)}^{trans})} \quad [9]$$

Materials and Methods

Planar Lipid Membranes. Free-standing bilayer lipid membranes (BLM) were formed from proteoliposomes as described previously (33, 34). In brief, BLM were folded across an aperture (150–250 μm in diameter) from the monolayers, which formed spontaneously on top of the vesicle suspension (45). The septum was

pretreated with 0.5% hexadecane in hexane. The electrical membrane parameters (bilayer resistance and conductivity) were continuously monitored by a picoammeter (VA10, NPI Electronic) connected via Ag/AgCl electrodes situated in the aqueous compartments next to the membrane. The solutions contained 100 mM NaCl (Merck) and were buffered with 5 mM Mops (Fluka). For the experiments at pH 8.9, Mops was substituted for equal amounts of Tris (Sigma-Aldrich). Magnetic stirring bars agitated the bathing solutions on both sides of the lipid membrane. After a stable lipid bilayer was formed, NaHS (Sigma-Aldrich) was added to the *cis* side and the chamber was covered with a lid. As the seal was not perfectly tight, the actual H₂S concentration in the donating compartment was determined by conductivity measurements. Therefore, time-lapse experiments were performed in which the buffer solution was replaced by 5 mM imidazole.

Microelectrode Measurements. We monitored steady-state acidification induced by transmembrane H₂S flux adjacent to the membrane, as previously described for other weak acids (30). In brief, a pH microelectrode was moved perpendicularly to the lipid membrane by a micromanipulator (Narishige). The potential changes at the tip of the pH-sensor were recorded with a high input-resistance electrometer (model 6514, Keithley) connected to a personal computer. The microelectrodes were made of borosilicate glass capillaries (GB150F-10, Science Products) pulled to a tip diameter of 2–4 μm, silanized with Bis(dimethylamino)dimethylsilane (Fluka) and filled with a proton-sensitive mixture (Hydrogen Ionophore II mixture A, Selectophore, Fluka). All microelectrode measurements were carried out at 23 °C.

The experiments were done while continuously stirring the bulk solutions. The system would otherwise not have reached steady state within a reasonable amount of time. Because an exact analytical solution for the combined processes of convection, diffusion, and chemical reactions is not available for the geometry of the measurement chamber, we restricted the mathematical analyses to concentrations measured within the first 50 μm from the membrane. In this region, the stirring velocity is negligible small and transport is assumed to occur only by diffusion.

Protein Expression, Purification and Reconstitution. The AfAQP gene was amplified from a plasmid containing the *A. fulgidus* AfAQP gene, obtained from ATCC

(catalog no. 630307R) by PCR, and the *A. fulgidus* AQP gene was inserted into a pET28b expression vector (Novagen) with an *N*-terminal octahistidine (His-8)-affinity tag followed by a human rhinovirus 3C protease site. *E. coli* BL21(DE3)RIL cells (Stratagene) were transformed with the plasmid containing the AfAQP gene and plated on LB agar containing 50 μg/mL kanamycin and 35 μg/mL chloramphenicol. All cultures were grown in autoinduction LB media containing 50 μg/mL kanamycin and 35 μg/mL chloramphenicol at 37 °C in Fernbach flasks shaking at 200 rpm. For expression, each liter of growth media was inoculated with 25 mL of an overnight culture started from a freshly transformed colony and allowed to grow for 16 h. The cells were harvested by centrifugation for 15 min at 5,000 × *g* and 4 °C. The pelleted cells were resuspended in 50 mM Tris (pH 7.4), 500 mM NaCl, 5 mM EDTA and 1 mM PMSF, and lysed with 3–5 passages at 15,000 psi in an EmulsiFlex-C5 high-pressure homogenizer (Avestin). The membranes were pelleted by ultracentrifugation at 160,000 × *g* for 1 h (at 4 °C). The membrane was immediately resuspended in solubilization buffer containing 50 mM Tris (pH 7.4), 200 mM NaCl, 10% (vol/vol) glycerol. The protein was solubilized by adding octyl-β-D-glucopyranoside (OG, Anatrace) to a final concentration of 5% to the resuspended membranes and stirred at 4 °C for 3 h. Unsolubilized material was pelleted by ultracentrifugation at 160,000 × *g* for 1 h at 4 °C. The supernatant was loaded onto a column containing 3–5 mL of nickel-nitrilotriacetic acid (Ni-NTA) resin (Qiagen), washed consecutively with a wash buffer (50 mM Tris (pH 7.4), 300 mM NaCl, 10% (vol/vol) glycerol, 40 mM imidazole, 1.2% OG), and then eluted with same buffer containing 300 mM imidazole. Imidazole was removed by using an Econo-Pac DG10 desalting column (Bio-Rad). The histidine affinity tag was removed by using excess 3C protease at room temperature for 12–16 h. The final protein-purification step was achieved by size-exclusion chromatography on a Superdex 200 column (GE Biosciences) in 50 mM Tris, pH 7.4, 200 mM NaCl, 1.2% OG and 10% (vol/vol) glycerol. The purity of the preparation was checked by Coomassie staining (Fig. S3). Protein reconstitution into proteoliposomes was generally performed as previously described (15).

ACKNOWLEDGMENTS. We thank Quentina Beatty for proofreading the manuscript. This project was supported by Austrian Science Fund Grant FWF W1201-N13 (to P.P.) and National Institutes of Health Grants DK43955 and DK048217 (to M.Z.L. and J.C.M.).

1. Lefer DJ (2007) A new gaseous signaling molecule emerges: Cardioprotective role of hydrogen sulfide. *Proc Natl Acad Sci USA* 104:17907–17908.
2. Zhao W, Zhang J, Lu Y, Wang R (2001) The vasorelaxant effect of H₂S as a novel endogenous gaseous K_{ATP} channel opener. *EMBO J* 20:6008–6016.
3. Pryor WA, et al. (2006) Free radical biology and medicine: It's a gas, man! *Am J Physiol Regul Integr Comp Physiol* 291:R491–R511.
4. Elrod JW, et al. (2007) Hydrogen sulfide attenuates myocardial ischemia-reperfusion injury by preservation of mitochondrial function. *Proc Natl Acad Sci USA* 104:15560–15565.
5. Yang G, et al. (2008) H₂S as a physiologic vasorelaxant: Hypertension in mice with deletion of cystathionine gamma-lyase. *Science* 322:587–590.
6. Li L, et al. (2005) Hydrogen sulfide is a novel mediator of lipopolysaccharide-induced inflammation in the mouse. *FASEB J* 19:1196–1198.
7. Zanardo RCO, et al. (2006) Hydrogen sulfide is an endogenous modulator of leukocyte-mediated inflammation. *FASEB J* 20:2118–2120.
8. Abe K, Kimura H (1996) The possible role of hydrogen sulfide as an endogenous neuro-modulator. *J Neurosci* 16:1066–1071.
9. Kamoun P (2004) Endogenous production of hydrogen sulfide in mammals. *Amino Acids* 26:243–254.
10. Boehning D, Snyder SH (2003) Novel neural modulators. *Annu Rev Neurosci* 26:105–131.
11. Reiffenstein, et al. (1992) Toxicology of hydrogen sulfide. *Annu Rev Pharmacol Toxicol* 32:109–134.
12. Li L, Moore PK (2008) Putative biological roles of hydrogen sulfide in health and disease: a breath of not so fresh air? *Trends Pharmacol Sci* 29:84–90.
13. Calhoun DB, Englander SW, Wright WW, Vanderkooi JM (1988) Quenching of room temperature protein phosphorescence by added small molecules. *Biochemistry* 27:8466–8474.
14. Deamer DW, Bramhall J (1986) Permeability of lipid bilayers to water and ionic solutes. *Chem Phys Lipids* 40:167–188.
15. Hub JK, et al. (2005) Structural basis for conductance by the archaeal aquaporin AqpM at 1.68 Å. *Proc Natl Acad Sci USA* 102:18932–18937.
16. Kozono D, et al. (2003) Functional expression and characterization of an archaeal aquaporin. AqpM from methanothermobacter marburgensis. *J Biol Chem* 278:10649–10656.
17. Boron WF (2006) Acid-base transport by the renal proximal tubule. *J Am Soc Nephrol* 17:2368–2382.
18. Saparov SM, Liu K, Agre P, Pohl P (2007) Fast and selective ammonia transport by aquaporin-8. *J Biol Chem* 282:5296–5301.
19. Herrera M, Hong NJ, Garvin JL (2006) Aquaporin-1 transports NO across cell membranes. *Hypertension* 48:157–164.
20. Hub JS, de Groot BL (2008) Mechanism of selectivity in aquaporins and aquaglyceroporins. *Proc Natl Acad Sci USA* 105:1198–1203.
21. Missner A, Pohl P (2009) 110 years of the Meyer-Overton rule: Predicting membrane permeability of gases and other small compounds. *ChemPhysChem* 10:1405–1414.
22. Missner A, et al. (2008) Carbon dioxide transport through membranes. *J Biol Chem* 283:25340–25347.
23. Sokolov VS, Pohl P (2009) Membrane transport of singlet oxygen monitored by dipole potential measurements. *Biophys J* 96:77–85.
24. Antonenko YN, Pohl P, Denisov GA (1997) Permeation of ammonia across bilayer lipid membranes studied by ammonium ion selective microelectrodes. *Biophys J* 72:2187–2195.
25. Al-Awqati Q (1999) One hundred years of membrane permeability: Does Overton still rule? *Nat Cell Biol* 1:E201–E202.
26. Saparov SM, Antonenko YN, Pohl P (2006) A new model of weak acid permeation through membranes revisited: Does Overton still rule? *Biophys J* 90:L86–L88.
27. Barry PH, Diamond JM (1984) Effects of unstirred layers on membrane phenomena. *Physiol Rev* 64:763–872.
28. Pohl P, Saparov SM, Antonenko YN (1998) The size of the unstirred layer as a function of the solute diffusion coefficient. *Biophys J* 75:1403–1409.
29. Walter A, Gutknecht J (1986) Permeabilities of small nonelectrolytes through lipid bilayer membranes. *J Membr Biol* 90:207–217.
30. Antonenko YN, Denisov GA, Pohl P (1993) Weak acid transport across bilayer lipid membrane in the presence of buffers—Theoretical and experimental pH profiles in the unstirred region. *Biophys J* 64:1701–1710.
31. Krylov AV, Pohl P, Zeidel ML, Hill WG (2001) Water permeability of asymmetric planar lipid bilayers: Leaflets of different composition offer independent and additive resistances to permeation. *J Gen Physiol* 118:333–340.
32. Lande MB, Donovan JM, Zeidel ML (1995) The relationship between membrane fluidity and permeabilities to water, solutes, ammonia, and protons. *J Gen Physiol* 106:67–84.
33. Pohl P, Saparov SM, Borgnia MJ, Agre P (2001) High selectivity of water channel activity measured by voltage clamp: Analysis of planar lipid bilayers reconstituted with purified AqpZ. *Proc Natl Acad Sci USA* 98:9624–9629.
34. Saparov SM, Kozono D, Rothe U, Agre P, Pohl P (2001) Water and ion permeation of aquaporin-1 in planar lipid bilayers: Major differences in structural determinants and stoichiometry. *J Biol Chem* 276:31515–31520.
35. Subczynski WK, Hyde JS, Kusumi A (1989) Oxygen permeability of phosphatidylcholine-cholesterol membranes. *Proc Natl Acad Sci USA* 86:4474–4478.
36. Dzikovski BG, Livshits VA, Marsh D (2003) Oxygen permeation profile in lipid membranes: Comparison with transmembrane polarity profile. *Biophys J* 85:1005–1012.
37. Mathai JC, Sprott GD, Zeidel ML (2001) Molecular mechanisms of water and solute transport across archaeobacterial lipid membranes. *J Biol Chem* 276:27266–27271.
38. Illsley NP, Verkman AS (1986) Serial permeability barriers to water transport in human placental vesicles. *J Membr Biol* 94:267–278.
39. Pohl P, Saparov SM (2000) Solvent drag across gramicidin channels demonstrated by microelectrodes. *Biophys J* 78:2426–2434.
40. Mathai JC, Tristram-Nagle S, Nagle JF, Zeidel ML (2008) Structural determinants of water permeability through the lipid membrane. *J Gen Physiol* 131:69–76.
41. Nagle JF, Mathai JC, Zeidel ML, Tristram-Nagle S (2008) Theory of passive permeability through lipid bilayers. *J Gen Physiol* 131:77–85.
42. Ehring GR, Zampighi G, Horwitz J, Bok D, Hall JE (1990) Properties of channels reconstituted from the major intrinsic protein of lens fiber membranes. *J Gen Physiol* 96:631–664.
43. Simon SA, Gutknecht J (1980) Solubility of carbon dioxide in lipid bilayer membranes and organic solvents. *Biochim Biophys Acta* 596:352–358.
44. Gutman M, Nachliel E (1997) Time-resolved dynamics of proton transfer in proteinous systems. *Annu Rev Phys Chem* 48:329–356.
45. Schindler H (1989) Planar lipid-protein membranes: strategies of formation and of detecting dependencies of ion transport functions on membrane conditions. *Methods Enzymol* 171:225–253.
46. Tamimi A, Rinker EB, Sandall OC (1994) Diffusion-coefficients for hydrogen-sulfide, carbon-dioxide, and nitrous-oxide in water over the temperature-range 293–368-K *J Chem Eng Data* 39:330–332.